Electronic Supplementary Information

Covalent Organic Frameworks as Micro-reactors: Confinement-enhanced Electrochemiluminescence

Wei-Jia Zeng[†‡], Kun Wang[†], Wen-Bin Liang[†], Ya-Qin Chai[†], Ruo Yuan[†], Ying Zhuo[*,†]

[†] *Chongqing Engineering Laboratory of Nanomaterials & Sensor Technologies, College of Chemistry and Chemical Engineering, Southwest University, Chongqing 400715, China*

[‡] *National Engineering Research Center for Modernization of Traditional Chinese Medicine - Hakka Medical Resources Branch, College of pharmacy, Gannan Medical University, Ganzhou 341000, China*

[*] Corresponding authors: Tel.: +86 23 68252277, fax: +86 23 68253172.

E-mail addresses: yingzhuo@swu.edu.cn (Y. Zhuo).

Table of Contents

1. Experimental Section

Reagents and material. Tris-(2,2-bipyridyl) Ruthenium (II) chloride hexahydrate ($Ru(bpy)_3^{2+}$) was bought from Suna Tech Inc. (Suzhou, China). 1,3,5-triformylbenzene was received from Ark Pharm Inc. (Chicago, America). 1,4-diaminobenzene was obtained from Aladdin Co. (Shanghai, China). Hexanethiol (HT, 96%), kanamycin, nafion (5 wt%), Poly-(diallyldimethylammonium chloride) (PDDA), sodium borohydride ($NaBH_4$), potassium ferricyanide [$K_4Fe(CN)_6$], gold chloride tetrahydrate ($HAuCl_4 \cdot 4H_2O$, 99.9%), hexachloroplatinic (H_2PtCl_6), glycine were purchased from Sigma-Aldrich Co. (St. Louis., MO., USA). The aflatoxin M1 (AFM1, 98%), aflatoxin B1 (AFB1, 98%) and aflatoxin B2 (AFB2, 98%) were bought from J & K Scientific Co., Ltd. (Beijing, China). Ferric chloride ($FeCl_3 \cdot 6H_2O$) was bought from Qiangshun Chemical Reagent Co. Ltd. (Shanghai, China). Poly(vinylpyrrolidone) (PVP, MW=30000), aqueous acetic acid, tetrahydrofuran, N, N-dimethylformamide, ethanol and 1,4-dioxane and tripropylamine (TPrA) were provided by Chengdu Chemical Reagent Co. (Chengdu, China). Nt. BbvCI restriction endonuclease, 10 × Cutsmart Buffer, T7 exonuclease (T7 Exo) and 10 × NE buffer were bought from New England Biolabs, Inc. (Beverly, MA, USA). All DNA strands with sequences in the Table S1 were received from Sangon Biotech Co., Ltd. (Shanghai, China).

Table S1. Sequence information for the nucleic acids used in this study

Name	Sequence* (5'– 3')
S0	CAA ATA ACA CTC ATT CTT AG GA AC CCTCAGC TTC TTA TTTTTT-$(CH_2)_6$-NH_2
Walker	GCT GAG GGT ACT GCT AGA GAT TTT CCA CAT CTC CTA ACA ATT GCT GAC CTC GCT GAG GGT TCT AGC AGT ACC
S1	GGT TCC TAA GAA T GAG TGT TAC TAT CAT T -$(CH_2)_6$-NH_2
S2	Fc- ATG ATA GTA ACA CTC A T

The buffers involved in this work were used as follows: 1×TE buffer (10 mM Tris–HCl, 1.0 mM ethylene diaminetetraacetic acid (EDTA), pH 8.0), DNA hybridization buffer (HB) (10 mM Tris-HCl, 1.0 mM EDTA, 1.0 M NaCl, pH 7.0), Phosphate buffer saline (PBS) (0.1 M Na_2HPO_4, 0.1 M KH_2PO_4 and 0.1 M KCl, pH 7.4). Besides, deionized water was used throughout the experiment. The gold nanoparticles (AuNPs) was prepared by citrate reduction of $HAuCl_4 \cdot 4H_2O$ according to the classic procedure.[1]

Apparatus. The ECL response was recorded by an MPI-E multifunctional analyzer (Xi'an Remax Electronic Science & Technology Co. Ltd., Xi'an, China). The working potential was from 0 to 1.1 V at a scan rate 0.3 V/s in the process of ECL detection. Measurements were performed using conventional three-electrode system (a platinum wire as counter electrode, a modified glass carbon electrode (GCE, Φ = 4mm) as working electrode, and Ag/AgCl (saturated KCl) as reference electrode). The cyclic voltammetry (CV) were implemented with a CHI 660C Electrochemistry Workstation (Shanghai CH Instruments, China). The morphologies of the nanomaterials were characterized by using a scanning electron microscope (SEM, S-4800, Hitachi, Tokyo, Japan) and transmission electron microscope (TEM,

H600, Hitachi, Tokyo, Japan). X-ray diffraction (XRD, BRUCKER D8, Germany) was utilized for the characterization of the as-prepared nanomaterials. Zeta potentials are measured by dynamic laser light scattering (ZEN3600, Malvern).

Synthesis of COF-LZU1. A facile and fast approach was developed to synthesize COF-LZU1 according to the previous literature with some modifications.[2] Firstly, 1,4-diaminobenzene (8 mg) and 1,3,5-triformylbenzene (8 mg) were fully dissolved in 1 mL 1,4-dioxane. Subsequently, 0.1 mL aqueous acetic acid (3 M) was added to the above mixture to produce a lot of yellow precipitates (COF-LZU1) immediately. After the above mixture left undisturbed for 30 min at the room temperature, the yellow precipitates were washed with tetrahydrofuran and *N, N*-dimethylformamide for three times, respectively. Next, the COF-LZU1 was collected by centrifugation, vacuum dried at 60 °C for 12 h and has been in storage at the room temperature for further use.

Synthesis of Ru@COF-LZU1 composites. To prepare the Ru@COF-LZU1 composites, nafion was used as crosslinker to modify the surface of COF-LZU1 with negative charges. Firstly, 0.3 mg COF-LZU1 was first dispersed in 3 mL nafion ethanol solution (2 wt%) by ultrasonic dispersion. To obtain Ru@COF-LZU1 composites, 100 μL $Ru(bpy)_3^{2+}$ (25 mM) was injected into the resultant solution under stirring for 30 min at 25 ℃. Then, the Ru@COF-LZU1 composites were washed several times to remove the free $Ru(bpy)_3^{2+}$, and the obtained Ru@COF-LZU1 composites were collected after centrifugation at 12,000 rpm for 10 minutes. Finally, the precipitationwascollected and resuspended in 5 mL 0.1 M PBS and stored at 4 °C

for further use.

Synthesis of Pt Concave Nanocubes. The Pt concave nanocubes (Pt CNCs) were synthesized according to previous report with some modification.[3] Firstly, PVP (MW = 40000, 0.2g), glycine (75 mg) and H_2PtCl_6 solution (1mL, 20 mM) were added to 3 mL deionized water and stirred for 5 min at 25 °C. Then the resultant yellow homogeneous solution was transferred to a 20 mL Teflon-lined stainless-steel autoclave and placed in an oven at 200 °C for 6 h. Finally, the products were collected by centrifugation at 11 000 rpm for 20 min and washed with ethanol for 3 times, and then re-dispersed in 10 mL deionized water and stored at 4 °C for further use.

Synthesis of Au@Fe_3O_4. The Au@Fe_3O_4 was synthesized according to previous report with some modification.[4] Briefly, 10 mL of 0.4 mM $NaBH_4$ aqueous solutions was dropped cautiously and slowly into 30 mL solution of 14 mM $FeCl_3 \cdot 6H_2O$ under stirring by hand at room temperature. With the addition of $NaBH_4$ solutions, a lot of black precipitates of Fe_3O_4 nanoparticles could be observed in the above solution. And then, the Fe_3O_4 was collected and washed with deionized water and ethanol for 3 times. Subsequently, 5.0 mg Fe_3O_4 was added into 5 mL 1 wt % PDDA aqueous solution, followed by shaking for 12 h at room temperature with shaker rate at 100 r/min. After centrifugation for removing excess PDDA, 1 mL AuNPs solution was added into the above solution (PDDA@Fe_3O_4) to prepare AuNPs coated Fe_3O_4 composite (Au@Fe_3O_4) under shaking for 4 h at room temperature. Ultimately, Au@Fe_3O_4 composite was washed 3 times and stored at 4 °C for further use.

Procedure of AFM1 conversion strategy. To convert the AFM1 to output

DNA, the magnetic probes were prepared in advance. Specifically, 10 μL support probe S0 (2 μM) was fully mixed with 10 μL Au nanoparticles modified Fe_3O_4 nanoparticles (Au@Fe_3O_4 NPs) solution for 12 h under stirring and magnetically separating to achieve the S0-Au@Fe_3O_4 (the preparation and the morphology characterization of Au@Fe_3O_4 NPs were shown in Section 2 of the supplementary material). Then, the mixture comprised of 5 μL AFM1 standard/sample solution and 5 μL walker (4 μM, hairpin probe) was incubated with S0-Au@Fe_3O_4 solutionfor 2 h at 37 °C. Herein, the AFM1 could open the walker by aptamer recognition to release the two legs of the walker. Next, the two legs of the walker paired with the S0 to produce a recognition site to generate massive of output DNA, in the presence of 200 U/mL Nt.BbvCI restriction endonuclease. After magnetic separation, plenty of output DNA was obtained for further detection.

Procedure of biosensor preparation and ECL detection. The used glass carbon electrode (GCE) was pretreated according to the previous literature.[5] Then, 5 μL Ru@COF-LZU1 solution was dropped onto the resultant GCE and let it dry in the air. Subsequently, 10 μL solution of Pt CNCs was dropped onto the Ru@COF-LZU1/GCE through electrostatic interaction. Next, 10 μL 2 μM amino-modified S1 was immobilized on the electrode surface through Pt-N bonds for 12 h at 4 °C. Then, 10 μL Fc-labeled S2 (2 μM) was dropped onto the Pt CNCs/Ru@COF-LZU1/GCE for 2 h at 25 °C to form dsDNA S1-S2 for quenching the ECL signal of Ru@COF-LZU1 by Fc. Finally, the resultant electrode was was immersed in hexanethiol solution (HT, 1 mM) for 50 min at 25 °C, and the ECL and cyclic voltammetry (CV)

characteristics of the proposed biosensor were shown in Section 3 of the supplementary material.

After rinsing thoroughly with deionized water, 10 μL mixed solution (containing 5 μL output DNA, 5 μL T7 Exo in 1 × NE buffer) was incubated with the proposed biosensor for 2 h at 25 °C, which was washed with deionized water thoroughly. The ECL measurements were performed on MPI-E multifunctional analyzer with the potential ranged from 0 to 1.1 V at a scan rate of 300 mV/s in 2 mL PBS containing 5 mM TPrA.

2. SEM characterization of Pt CNCs and Au@Fe_3O_4

SEM was used to characterize the morphologies and sizes of Pt CNCs, as shown in Fig. S1A, the SEM image of synthesized Pt CNCs exhibited a uniform concave cube with an average size of approximately 50 nm, which was consistent with the reported literature.[3] According to the SEM image of Fig. S1B, the Fe_3O_4 exhibited a sphere shape, besides, the Au nanoparticles with the size about 10 nm were unevenly distributed in the surface of Au@Fe_3O_4.

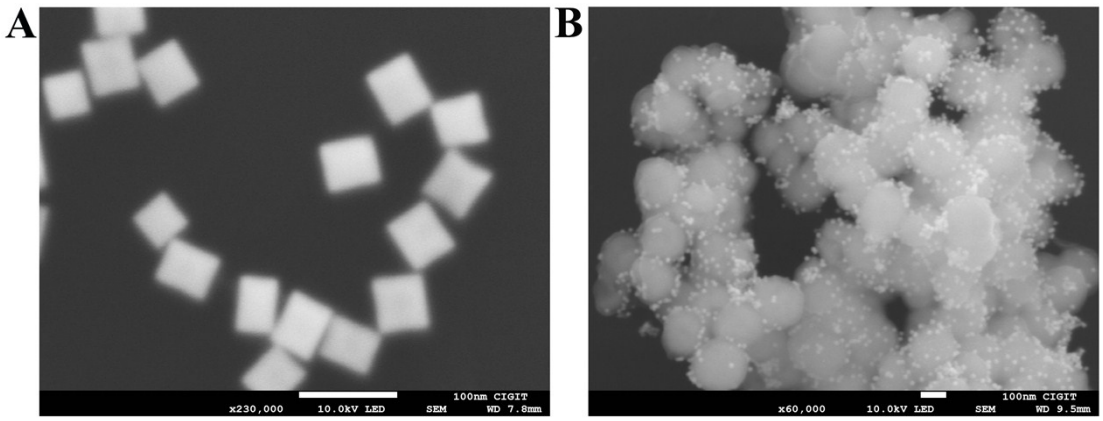

Figure S1 SEM image of Pt CNCs (A) and Au@Fe_3O_4 (B)

3. Zeta potential characterization of various COF-LZU1

Zeta potential is a common method to verify the nanomaterial surface charge. The zeta potential of COF-LZU1, nafion assembled imine-linked COFs (nafion@COF-LZU), $Ru(bpy)_3^{2+}$ assembled imine-linked COFs (Ru@COF-LZU1) were measured at pH=7.4, respectively, and the related data was displayed in Fig. S2. Zeta potential value of COF-LZU1 was about 8.0 mV, indicating that COF-LZU1 were positively charged. And the zeta potential values of nafion@COF-LZU1 was about -49.7 mV, which attributed to the effect of anionic polymer nafion. The zeta potential value increased to -32.7 mV when the $Ru(bpy)_3^{2+}$ was adsorbed to the surface of nafion@COF-LZU1 through the electrostatic interaction.

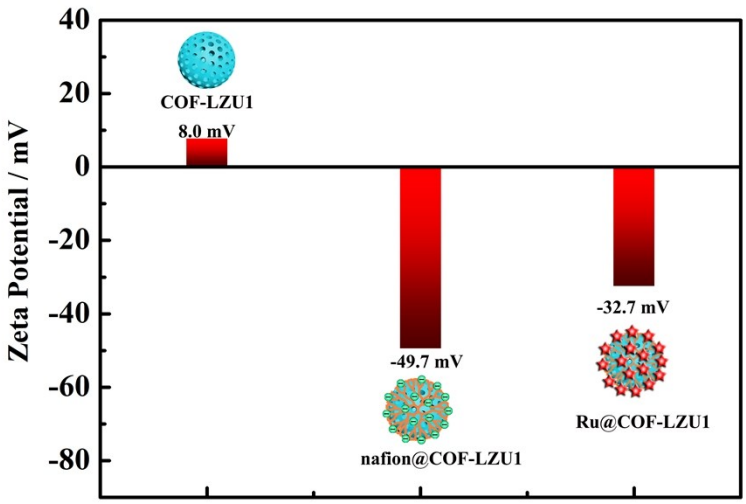

Figure S2: the zeta potential of the COF-LZU1, nafion@COF-LZU1 and the Ru@COF-LZU1

4 The effect of the dissolved oxygen on the stability of TPrA•

To further investigate the COF-LZU1 as the micro-reactors could reduce the effect of the dissolved oxygen on the stability of TPrA•. The CV curves of GCE and the COF-LZU1/GCE were recorded in TPrA solution under the aerobic and anaerobic

conditions, respectively. As shown in the Fig. S3, an anodic peak was observed at the GCE in the TPrA solution under anaerobic condition (curve *a*), which attributed to the electro-oxidation of TPrA.[6] When the GCE was measured in the air-saturated TPrA solution, the oxidation current of TPrA solution (curve *b*) decreased a lot compared with that of in the deoxidized TPrA solution (curve *a*), indicating that the dissolved oxygen could significantly affect the oxidation of TPrA. The main cause was that the dissolved oxygen could consume a large amount of the TPrA intermediate radical ($TPrA^{\bullet}$).[7] Surprisingly, when the COF-LZU1/GCE was measured in the air-statured TPrA solution, the oxidation current (curve *c*) increased apparently in comparison with the peak current of GCE in the same solution (curve *b*), demonstrating that the COF-LZU1 could reduce the impact of the dissolved oxygen on the oxidation of TPrA effectively. The possible reason was that the COF-LZU1 with hydrophobic porous nanochannels as the micro-reactors could not only provide a relatively independent and confined reaction environment for the electrochemical oxidation of TPrA, but also shield the quenching effect of dissolved oxygen on the $TPrA^{\bullet}$. When the COF-LZU1/GCE was measured in the TPrA solution under deoxidized condition, the oxidation current showed little growth compared with the oxidation current of GCE in TPrA solution under (curve *a*) deoxidized condition, because the COF-LZU1 as the micro-reactors could improve the oxidation efficiency of TPrA *via* concentrating the TPrA from the solution. These phenomena demonstrated that the existence of the COF-LZU1 micro-reactors could significantly improve the oxidation efficiency of TPrA and caused more $TPrA^{\bullet}$ in the $Ru(bpy)_3^{2+}$/TPrA system.

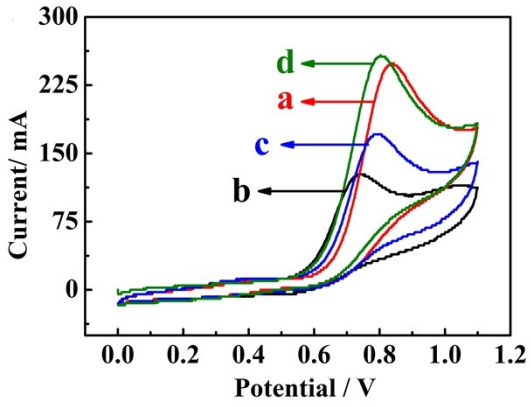

Fig.S3 The CVs of GCE in the 0.1 M $C_2H_3N/C_{16}H_{36}BF_4N$ solution containing 5 mmol/L TPrA before (b) and after deaeration (a), the CVs of COF-LZU1/GCE in the 0.1 M $C_2H_3N/C_{16}H_{36}BF_4N$ solution containing 5 mM TPrA before (c) and after deaeration (d).

5. ECL and CV Characteristics of the Proposed Biosensor

To identify the successful fabrication of the aptasesnor, the ECL measurements were performed in 2 mL PBS (PH=7.4) containing 5 mM TPrA to monitor the changes of electrode surface. As shown in Fig. S4A, no ECL response was observed when the GCE was measured in 2 mL PBS (PH=7.4) containing 5 mM TPrA (curve *a*). As expected, when the Ru@COF-LZU1 composite was dropped on the GCE, a strong signal of 11669 a.u. (curve *b*) was observed, which was attributed to the transition of the excited state of $Ru(bpy)_3^{2+*}$.[8] After the Pt CNCs was dropped onto the above electrode, the ECL responses achieved to the maximum of 12421 a.u. (curve *c*), demonstrating that Pt CNCs provide a higher effective electrochemical surface area and promoted the electron transfer. Then the ECL signal dropped markedly (curve *d*) after the dsDNA S1-S2 was immobilized on the modified

electrode surface, owing to the quenching effect of Fc-labeled S2 on $Ru(bpy)_3^{2+}$/TPrA ECL system. After the result electrode was blocked with HT, the ECL signal was further decreased (curve *e*). The ECL signal was increased abruptly to 10737 a.u. when the output DNA and T7 Exo were introduced onto the electrode surface, the reason could be that T7 Exo could cleave the S1-S2-T duplex from blunt or recessed 5'-termini to remove ferrocene for the ECL signal recovery.

The CV method was further employed to monitor the construction process of the modified electrode at every step in 2 mL PBS containing 5.0 mM $[Fe(CN)_6]^{3-/4-}$. As shown in Fig. S4B, a couple of reversible redox peaks was displayed on the bare GCE (curve *a*). The peak current decreased (curve *b*) when Ru@COF-LZU1 composite was dropped on the bare GCE, because the Ru@COF-LZU1 impeded the transmission of electrons. The peak current increased a lot (curve *c*) when the Pt CNCs was dropped on the modified electrode. The peak current decreased (curve *d*) when the dsDNA S1-S2 was immobilized onto the electrode surface by Pt-N bonds, this result could be the fact that the dsDNA inhibited the interfacial electron transfer. Then the peak current further decreased (curve *e*) after the HT blocked the nonspecific adsorption sites. Finally, after the output DNA and T7 Exo were incubated with the resultant electrode surface, the peak current increased abruptly for the reason that T7 Exo could cleave the S1-S2-output DNA duplex from blunt or recessed 5'-termini to remove a large amount of DNA from the electrode. All these results suggested that the proposed ECL aptasensor was successfully constructed.

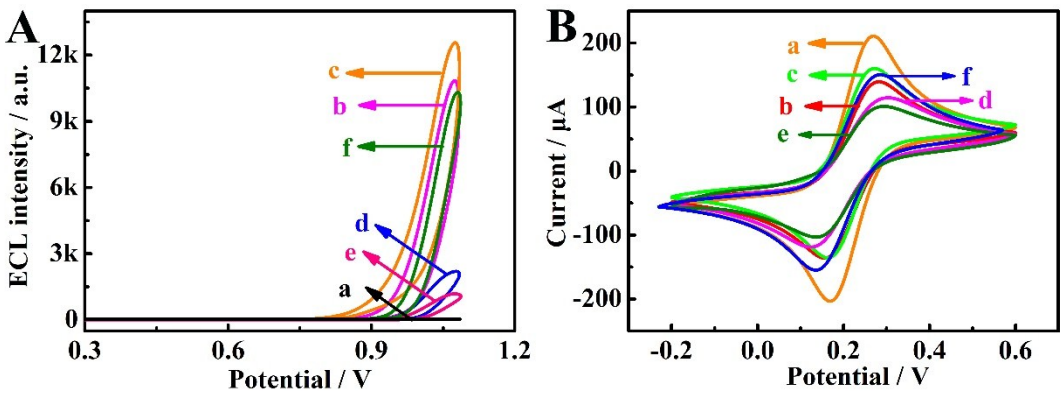

Figure S4. ECL curves in PBS containing 5 mM TPrA (A) and CV curves in PBS containing 5.0 mM $[Fe(CN)_6]^{3-/4-}$ of different modified electrodes. (a) GCE, (b) Ru@COF-LZU1/GCE, (c) Pt CNCs/ Ru@COF-LZU1/GCE, (d) dsDNA S1-S2/Pt CNCs/Ru@COF-LZU1/GCE, (e) HT/dsDNA S1-S2/Pt CNCs/ Ru@COF-LZU1/GCE, (f) the prepared HT/dsDNA S1-S2/Pt CNCs/ Ru@COF-LZU1/GCE complementary intermediated output DNA incubated with T7 Exo.

6 The calculation procedure of the LOD

The LOD was calculated with the traditional and typical approach reported in the previous references.[9-10] An ECL measurement for blank samples was executed with three parallel tests, which exhibited average ECL intensity (IB) of 960 a.u. with standard deviation (SB) of 35.1. To calculate the LOD, with signal-to-noise ratio value (k1) of 3, the smallest detectable signal could be calculated as

$$I_L = I_B + k_1 S_B = 1065.3$$

According to the linear regression equation I = 1279.62 lg c +3624.45, the LOD could be calculated as 0.009 pg/mL.

7 Table S2

Table S2. Comparison of our ECL method with other methods in AFM1 detection

Measurement technique	Linear range	Detection limit	Reference
ECL aptasensor	5 ~ 150 ng mL^{-1}	0.01 ng mL^{-1}	11
Fluorescence aptasensor	0.005 ~ 0.15 pg mL^{-1}	1.5 $\times 10^{-3}$ ng mL^{-1}	12
Electrochemical aptasensor	0.01 ~ 0.1ng mL^{-1}	1.98$\times 10^{-3}$ ng mL^{-1}	13
ECL immunosensor	10^{-3} ~100 ng mL^{-1}	3$\times 10^{-4}$ ng mL^{-1}	14
ECL aptasensor	5$\times 10^{-5}$ ~ 0.1 ng L^{-1}	2$\times 10^{-5}$ ng mL^{-1}	15
ECL aptasensor	5$\times 10^{-5}$ ~ 300 ng mL^{-1}	9 $\times 10^{-6}$ pg mL^{-1}	This work

Reference

1 B.V. Enustun, J.J. Turkevich, *J. Am. Chem. Soc.,* 1963, **85,** 3317–3328.

2 S. Y. Ding, J. Gao, Q. Wang, Y. Zhang, W. G. Song, C. Y. Su, W. Wang, J. Am. *Chem. Soc.,* 2011, **133,** 19816-19822.

3 Z. C. Zhang, J. F. Hui, Z. C. Liu, X. Zhang, J. Zhuang, X. Wang, *Langmuir.* 2012, **28,** 14845-14848.

4 Z. H. Ai, L. R. Lu, J. P. Li, L. Z. Zhang, J. R. Qiu, M. H. Wu, *J. Phys. Chem. C.,* 2007, **111,** 4087-4093.

5 Y. Zhuo, N. Liao, Y. Q. Chai, G. F. Gui, M. Zhao, J. Han, Y. Xiang, R. Yuan, *Anal. Chem.,* 2014, 86, 1053-1060.

6 L. L. Li, Y. Chen, J. J. Zhu, *Anal. Chem.,* 2017, **89,** 358-371.

7 M. Hesari, M. S. Workentin, Z. F. Ding, *Chem. Sci.,* 2014, **5,** 3814-3822.

8 W. J. Miao, J. P. Choi, A. J. Bard, *J. Am. Chem. Soc.,* 2002, **124,** 14478-14485.

9 G. Long, J. Winefordner, *Anal. Chem.,* 1983, **55,** 712A-724A.

10 V. Zamolo, G. Valenti, E. Venturelli, O. Chaloin, M. Marcaccio, S. Boscolo, M. Poli, *ACS Nano,* 2012, **6,** 7989-7997.

11 S. M. Khoshfetrat, H. Bagheri, M. A. Mehrgardi, *Biosens. Bioelectron.,* 2018, **100,** 382-388.

12 H. Li, D. B. Yang, P. W. Li, Q. Zhang, W. Zhang, X. X. Ding, J. Mao, J. Wu, *Toxins*. 2017, **9,** 318.

13 B. H. Nguyen, D. L. Tran, Q. P. Do, H. L. Nguyen, N. H. Tran, P. X. Nguyen, *Mater. Sci. Eng. C.,* 2013, **33,** 2229-2234.

14 N. Gan, J. Zhou, P. Xiong, F. T. Hu, Y. T. Cao, T. T. Li, Q. L. Jiang. *Toxins.* 2013, **5,** 865-883.

15 J. L. Liu, M. Zhao, Y. Zhuo, Y. Q. Chai, R. Yuan, *Chem.-Eur. J*., 2017, **23,** 1853-1859.